

Entanglement dynamics of random quantum channels

Zhi Li,¹ Shengqi Sang,^{1,2} and Timothy H. Hsieh¹

¹*Perimeter Institute for Theoretical Physics, Waterloo, Ontario N2L 2Y5, Canada*

²*Department of Physics and Astronomy, University of Waterloo, Waterloo, Ontario N2L 3G1, Canada*

The process by which open quantum systems thermalize with an environment is both of fundamental interest and relevant to noisy quantum devices. As a minimal model of this process, we consider a qudit chain evolving under local random unitaries and local depolarization channels. After mapping to a statistical mechanics model, the depolarization acts like a symmetry-breaking field, and we argue that it causes the system to thermalize within a time scale independent of system size. We show that various bipartite entanglement measures—mutual information, operator entanglement, and entanglement negativity—grow at a speed proportional to the size of the bipartition boundary. As a result, these entanglement measures obey an area law: their maximal value during the dynamics is bounded by the boundary instead of the volume. In contrast, if the depolarization only acts at the system boundary, then the maximum value of the entanglement measures obeys a volume law. We complement our analysis with scalable simulations involving Clifford gates, for both one and two-dimensional systems.

INTRODUCTION

A quantum system interacting with an environment generically thermalizes, and attempts toward understanding the details of such thermalizing dynamics have led to many different techniques and approaches [1–6]. Recent advances in quantum hardware have added further motivation to understand such dynamics, as physical systems inevitably evolve in the presence of noise and will decohere in the absence of fault tolerance. Determining if such noisy dynamics [7] offers a quantum advantage over classical simulation would benefit from an understanding of the dynamics, in particular the entanglement dynamics. If the mixed state of the system is not too highly entangled during the dynamics, then classical simulation approaches may be efficient [8–12].

Recently, random circuits have provided a fruitful approach for studying many-body quantum dynamics of closed systems [13]. As a toy model, generic unitary time evolution is represented by local random unitaries, which admit a mapping of the dynamics to a classical statistical mechanics model [14]. This allows one to calculate many essential features of many-body quantum dynamics such as entanglement growth [13], spectral form factors [15], out-of-time-ordered correlations [16], and operator growth [17]. The random circuit architecture can also be hybridized with other elements. For example, random circuits interspersed with measurement have been widely studied and yield fascinating phenomena [18–20].

In this work, we use the random circuit approach to study the dynamics of open quantum systems. Such an application has already led to valuable insights in different contexts, see for example [21–24]. As a minimal model for a one-dimensional quantum system inside an infinite-temperature bath, we consider a circuit with random local unitaries and local depolarization channels, which together lead to random local quantum channels. We are interested in how the system eventually reaches

equilibrium (in this case, a maximally mixed state). We map the system into a classical spin model, with spins valued in a permutation group. After the mapping, the effects of the environment (the depolarizing channels) manifest as a permutation symmetry-breaking field which polarizes the spins and makes the system short-range correlated, thus setting a system-size-independent time scale to reach equilibrium. More specifically, we use mutual information, operator entanglement, and entanglement negativity as diagnoses of correlations, and we study their time dependence. These quantities show linear growth at early time, then reach their peak values and eventually drop to zero. Importantly, regardless of the strength of depolarization, we argue based on the statistical mechanics model that the peak is reached at a system-size-independent time, and the initial linear growth slopes are upper bounded by the size of the partition boundary. As a result, the peak values obey an area law: they are upper bounded by the size of the partition boundary as opposed to volume.

This setup was considered in Ref. [9], which reached the same conclusion for operator entanglement entropy based on numerics. Here, we provide analytic arguments for the above conclusion. For a complementary and scalable numerical simulation, we also consider a slightly different setup where the depolarization acts in a probabilistic fashion and the random unitaries are restricted to Clifford gates. Within this modified setup, we also find that the entanglement peaks obey an area law, for both one and two-dimensional systems. Finally, we also consider a model in which depolarization only occurs at the system boundary, and we find that the entanglement peaks obey volume law in this case, based on both analytical arguments and numerical calculations.

SETUP

We consider a one-dimensional qudit chain with local Hilbert space dimension d . The architecture is shown in Fig. 1(a), where blue blocks are random unitaries chosen independently and yellow strips are depolarizing channels. The combination of two types of blocks give the following random quantum channel:

$$\Phi(\rho) = (1-p)U\rho U^\dagger + \frac{p\text{tr}(\rho)}{d^2}\mathbb{I}. \quad (1)$$

Here U is a random unitary; \mathbb{I} is the maximally mixed state of two qudits; p is the strength of the depolarization. We choose the initial state to be a pure product state.

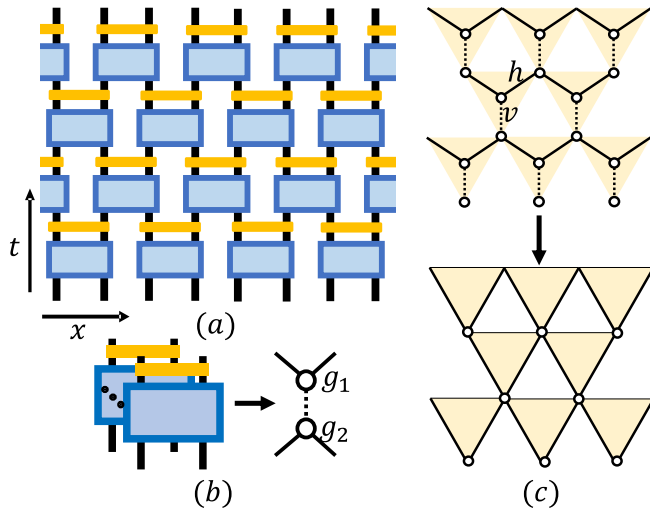


FIG. 1. (a) Architecture of the random circuit. Blue blocks are random unitaries and yellow strips are depolarizing channels with strength p . (b) Haar random average via Weingarten calculus. (c) After mapping to a spin model on honeycomb lattice, some spins are integrated out.

For concreteness, we will focus on the dynamics of the mutual information between two subsystems A and B :

$$I_n(A: B) = S_{n,A} + S_{n,B} - S_{n,AB}, \quad (2)$$

where $S_n(\rho) = \frac{1}{1-n} \log \text{tr} \rho^n$ ($n > 1$) is the Rényi entropy of ρ_A , ρ_B and ρ_{AB} . In [25] we also consider both entanglement negativity [26]—a mixed state entanglement measure, and operator entanglement entropy [27]—the complexity of representing the density matrix as a matrix product operator. We find similar behaviour for these quantities and thus focus on mutual information.

Due to the randomness in the model, I_n takes different values for each random circuit realization and corresponding trajectory ρ_t . We will be interested in the average over random circuit realizations:

$$\overline{I_n}(t) = \mathbb{E}[I_n(\rho_t)]. \quad (3)$$

To evaluate the average of logarithm, we will use the replica trick:

$$\mathbb{E} \log X = \frac{\partial}{\partial \alpha} \mathbb{E} X^\alpha \Big|_{\alpha=0}. \quad (4)$$

MAPPING TO STATISTICAL MECHANICS MODEL

Representing each ρ as a 2-layer circuit (legs live in H and H^* respectively) and taking Eq. (4) into consideration, terms in Eq. (2) are represented by multi-layer circuits, with legs on the boundary contracted suitably according to the trace and replica structure.

In the bulk, random channels at the same location (but different layers) are identical, while being independent of random channels at other locations. Each channel can be averaged independently using the Weingarten calculus, resulting in a summation over S_Q (the permutation group of Q elements, where Q is the number of layers divided by 2), see Fig. 1(b). The summations at all locations together can be regarded as a partition function of a classical spin model on a honeycomb lattice. On each lattice, there is an S_Q spin g ; the statistical weight for a spin configuration $\{g\}$ is:

$$\prod_v (1-p)^{Q-n_{g_1,g_2}} V_Q(g_1, g_2) \prod_h d^{-|g_1^{-1}g_2|}. \quad (5)$$

Here, v denotes vertical bonds and h denotes horizontal (zigzag) bonds [see Fig. 1(c)]; $|g|$ is the minimal number of transpositions in g ; n_{g_1,g_2} is the number of common *fixed points* of g_1 and g_2 . The coefficient $V_Q(g_1, g_2)$ is defined as

$$\sum_{i=0}^{n_{g_1,g_2}} \binom{n_{g_1,g_2}}{i} (1-p)^{n_{g_1,g_2}-i} p^i d^{2(Q-i)} W_{Q-i}(g_1^{-1}g_2), \quad (6)$$

where W_{Q-i} are the Weingarten functions, see [25] for details.

Following Ref. [14, 28, 29], we integrate out spins in the middle of triangles, resulting in a spin model on a (rotated) square lattice with the following triangle weights:

$$\begin{array}{c} b \\ \backslash \\ \triangle \\ / \\ a \end{array} = (1-p)^{Q-n_a} K_p(a, b, c), \quad (7)$$

where n_a is the number of fixed points of a and

$$K_p(a, b, c) = \sum_{\tau \in S_Q} d^{-|\tau^{-1}b| - |\tau^{-1}c|} (1-p)^{n_a - n_{\tau,a}} V_Q(\tau, a). \quad (8)$$

We comment on the symmetry. If $p = 0$, since both $W(\)$ and $|\ |$ are invariant under conjugation, the weights

have a $S_Q \times S_Q$ “spin rotation” symmetry acting as independent left/right group multiplication. If $p > 0$, the action must also keep various n_{g_1, g_2} and n_g invariant, hence only the diagonal S_Q group remains, acting by conjugation. In the case of $Q = 2$, the above statement should be slightly modified since S_2 has a nontrivial center (which is itself). The symmetry is S_2 (if $p = 0$) and $\{id\}$ (if $p > 0$).

The traces, which are suitable contractions on the top boundary (explicitly specified later), manifest as fixed boundary conditions in the spin model. The initial condition translates to a free boundary condition for our setup at the bottom boundary.

From Eq. (7) we can already see the effect of the depolarization in the spin model: the $(1-p)^{Q-n_a}$ factor favors spins with larger n_a . The depolarization acts as a polarizing field, which couples to the spins with energy $\propto -n_a$ and tries to polarize the spins to id . This field breaks the symmetry discussed above.

LARGE d ANALYSIS

We first analyze the $d = \infty$ limit. Here the triangle weights are:

$$\begin{array}{c} b \\ \backslash \quad / \\ \triangle \\ / \quad \backslash \\ c \\ \backslash \quad / \\ a \end{array} = \begin{cases} (1-p)^{Q-n_a}, & \text{if } a = b = c \\ 0, & \text{otherwise} \end{cases}. \quad (9)$$

Therefore all spins must be equal. If $p = 0$, the spins can take all possible directions, due to the mentioned symmetry; if $p > 0$, the symmetry breaks and spins are polarized to id .

For finite d , following Ref. [14], we visualize spin configurations in terms of domain wall configurations. There are $|a^{-1}b|$ domain walls across the edge $a-b$, each denoting a transposition in the decomposition of $a^{-1}b$. Working in the large d limit (only keep terms to the leading order in $\frac{1}{d}$), we calculate the triangle weights Eq. (7), see Tab. I for some examples. For the replica calculation,

$p \neq 0$	$(1-p)^{Q-n_a}$	$\frac{(1-p)^{Q-n_a}}{d}$	$(1-p)^{Q-n_a} \frac{1-(1-p)^{n_a-n_{a,c}}}{d^2}$
$p = 0$	1	$\frac{1}{d}$	0

TABLE I. Some triangle weights for the spin model. Here a, b, c is the spin on the bottom, left, right. In the second row we list $p = 0$ unitary-only case for comparison.

we also need multi-domain-wall triangles where all domain walls commute in S_Q [for example, (12) commutes with (34)]. It turns out that in all relevant cases and to the leading order, commuting domain walls contribute to the weights independently: the weight for a multi-domain-wall configuration equals the product of single

domain wall contributions indicated in Tab. I, see [25] for details.

As evident in Tab. I, besides the polarization effect of the $(1-p)^{Q-n_a}$ factor, the other effect of nonzero p is the existence of horizontal domain walls, with an extra penalty $\frac{1}{d}$ and an extra factor $1 - (1-p)^{n_a-n_{a,c}}$ to forbid them in the purely unitary case $p = 0$.

In the following, we focus on the second Renyi entropy I_2 and find

$$\begin{aligned} \overline{I_2} &= -2 \frac{\partial}{\partial Q} [\log \mathcal{Z}_{ba} + \log \mathcal{Z}_{ab} - \log \mathcal{Z}_{bb}] \\ &\approx -\log \mathcal{Z}_{ba} - \log \mathcal{Z}_{ab} + \log \mathcal{Z}_{bb} \Big|_{Q=2}. \end{aligned} \quad (10)$$

Here $a = id$ and $b = (1, 2)(3, 4) \cdots (Q-1, Q)$. The second line is due to the approximate independence mentioned above. $\mathcal{Z}_{g_1 g_2}$ denotes the partition function with spins above A region fixed to g_1 and spins above B region fixed to g_2 . \mathcal{Z}_{ab} comes from $\text{tr}(\rho_A^2)$ and \mathcal{Z}_{bb} comes from $\text{tr} \rho^2$; the latter also relates to the entropy of the whole system.

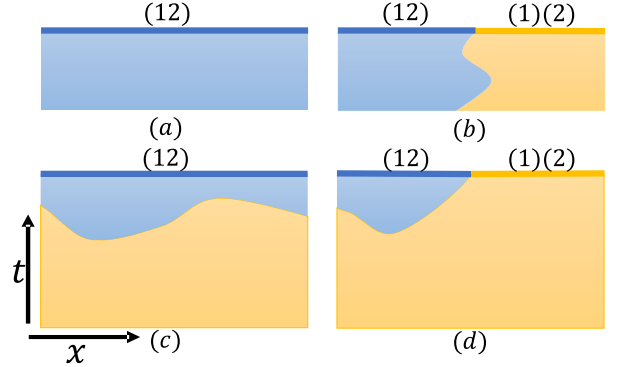


FIG. 2. Domain wall configuration for I_2 at (a)(b) small t and (c)(d) large t . The thick lines on the upper boundary indicate fixed boundary conditions corresponding to permutations. Yellow spins are $id = (1)(2)$; blue spins are (12) . The domain walls in (c)(d) are horizontally directed.

Spins near the upper boundary tend to be parallel to the fixed boundary conditions, while spins deep in the bulk tend to be polarized to id due to the polarization field. Therefore, which configurations dominate depends on the time t .

For small t , the dominant configurations are those with no domain walls or vertical domain walls only (due to the energy penalty $\frac{1}{d}$ for horizontal domain walls), see Fig. 2(a) for \mathcal{Z}_{bb} and Fig. 2(b) for \mathcal{Z}_{ba} . Assuming the cut is in the middle, we have

$$\mathcal{Z}_{bb} \approx (1-p)^{L t}, \quad (11)$$

since each triangle contributes a $(1-p)^2$ factor, and

$$\mathcal{Z}_{ab} = \mathcal{Z}_{ba} \approx \frac{2^t}{d^t} (1-p)^{\frac{L t}{2}} \prod_{i=1}^t \frac{(1-p)^{-i} + (1-p)^i}{2}. \quad (12)$$

Here, the factor $\frac{1}{d^t}$ is the energetic contribution from the domain wall; 2^t is roughly the entropic contribution (the domain wall can go left or right at each step). The number of non *id* spins depends on the domain wall, which gives the extra factor $\prod_{i=1}^t$, see [25] for details.

Eq. (10) now yields[30]:

$$\overline{I_2}(t) \approx (2 \log \frac{d}{2})t - 2 \sum_{i=1}^t \log \frac{(1-p)^{-i} + (1-p)^i}{2}. \quad (13)$$

Note that although both terms have an L dependence (the entropy of the system is extensive), they cancel exactly, resulting in a finite growth rate.

When t is large, the above configurations are not economical anymore. Instead, we need to consider domain walls separating the upper and lower boundaries, see Fig. 2(c)(d) for illustration. Interestingly, the sum over these fluctuating domain walls can be analytically carried out, under the restrictions that the number of domain walls is minimal (no “bubbles”) and *horizontally directed* (to keep the exponent of $\frac{1}{d}$ minimal). The method for the summation is iterative (over t or L), see [25] for details. Here we just mention that, as a sanity check, we find

$$\mathcal{Z}_{ab} \approx \mathcal{Z}_{bb} \approx \frac{1}{d^L} \quad (14)$$

for $t \rightarrow \infty$. This matches with the maximally mixed final state $\rho(t \rightarrow \infty) = \frac{\mathbb{I}}{d^L}$.

Comparing Eq. (11) and Eq. (12) with the infinite t result Eq. (14), we see there is a competition between $1/d$ and $(1-p)^t$, and equating them yields the timescale[31]

$$t^* = O\left(\frac{\log d}{-\log(1-p)}\right). \quad (15)$$

Vertical and horizontal domain walls dominate if $t < t^*$ and $t > t^*$ respectively. We emphasize that there is no L dependence in t^* .

AREA LAW

The system-size-independent growth rate in Eq. (13) can be regarded as an open system analog of the small incremental theorem [32, 33]. It can be rigorously proven for the von Neumann mutual information. Indeed, due to the monotonicity of the mutual information, $I(A:B)$ cannot increase under any quantum channels except those acting on the boundary, for which $I(A:B)$ at most increases by a constant each time step[25].

On the other hand, we also find that the system thermalizes in a system-size-independent timescale Eq. (15). From the statistical mechanics perspective, this reflects the fact that the fixed boundary condition has only short-range effects on the bulk spins. This is because the domain wall contribution $\sim \frac{1}{d^L}$ is boundary-like, but the

polarization field contribution $\sim (1-p)^{L^t}$ is extensive. Moreover, for $Q = 2$, the triangle weights in Tab. I can be equivalently summarized in terms of energies [up to $O(\frac{1}{d})$] as:

$$E = -\log d \sum_{\langle ij \rangle} (\delta_{\sigma_i \sigma_j} - 1) - \log \frac{1}{1-p} \sum_i (\delta_{\sigma_i} - 1), \quad (16)$$

which is the Ising model with a magnetic field on a (rotated) two-dimensional square lattice. The Gibbs state is well-known to be unique and short-range correlated for nonzero magnetic field (the same is true for more general models with a polarizing field like the Potts model [34, 35]).

Combining the above two facts, we arrive at an *area law*: the peak of mutual information is bounded by the boundary (hence “area”) instead of the volume.

NUMERICS

For a scalable simulation, we consider an alternative setup, see Fig. 3(a), where instead of a fixed strength p depolarizing channel, we apply with probability p a “trace channel” $\Phi_{\text{trace}}(\rho) = \frac{\text{tr}(\rho)}{d^2} \mathbb{I}$ on top of each unitary. We also restrict the random unitaries to Clifford gates. These modifications allow an effective simulation using the stabilizer formalism [36]. Both setups capture the dynamics of open quantum systems with strength $O(p)$ depolarization. Moreover, we can also map the new setup into a statistical mechanics model [25] with similar features as the previous model[37].

In Fig. 3, we show the dynamics of mutual information (equivalent to operator entanglement for stabilizer states) and entanglement negativity for different p and subsystem sizes $|A|$. It is clear that the peaks for both entanglement measures do not depend on the subsystem size and obey an area law. In fact, the entire dynamics for two different partitions $|A|=L/4, L/2$ ($L=256$) are nearly identical for $p=0.01$, see the top two curves of Fig. 3(b). In [25], we also consider a two-dimensional system evolving under random Clifford gates and depolarization, and the numerical results suggest that the area law still holds.

We note that area law in the new setup Fig. 3(a) implies area law in the previous setup Fig. 1(a) for any convex entanglement measure[38] \mathcal{M} . This is because a trajectory ρ_1 in the original setup Eq. (1) can be obtained by averaging trajectories ρ_2 in the new setup over the appearance of traces (the unitaries are fixed): $\rho_1 = \mathbb{E}_{\text{trace}}(\rho_2)$. Hence $\mathbb{E}\mathcal{M}(\rho_1) \leq \mathbb{E}\mathbb{E}_{\text{trace}}[\mathcal{M}(\rho_2)] = \mathbb{E}[\mathcal{M}(\rho_2)]$ due to the convexity of \mathcal{M} .

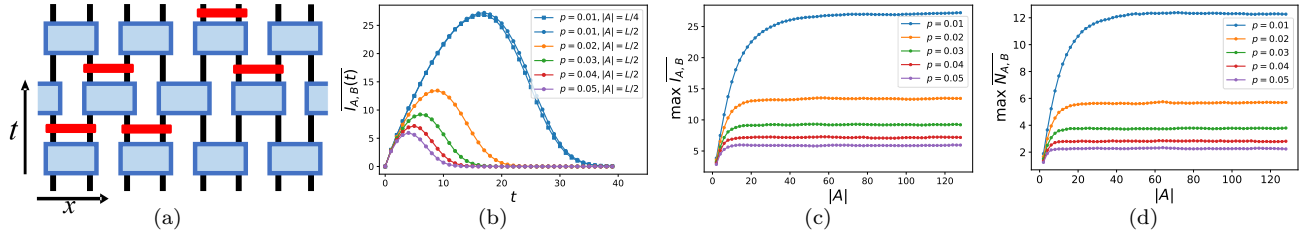


FIG. 3. (a) Architecture for the probabilistic trace setup. Trace channels (red strips) are applied with probability p after random Clifford unitaries. (b) Dynamics of bipartite mutual information for various p and $|A|$. (c) Maximum mutual information during the dynamics for various partitions $|A|$ and p . (d) Maximum log-negativity during the dynamics for various partitions $|A|$ and p . $L = 256$ in simulations above.

DISCUSSION

Using both an analytic mapping to a spin model and large scale Clifford simulations, we have argued that systems evolving under random unitaries and depolarization channels thermalize at an L -independent timescale Eq. (15), and correspondingly, entanglement measures such as mutual information, operator entanglement, and negativity have peaks obeying area laws. This implies, in addition to the evidence from Ref. [9], that matrix product operator simulations of such noisy 1d dynamics are in principle efficient, though in practice the required bond dimension may still be large when the noise strength p is small.

The L -independent timescale originates from the extensiveness of the depolarization. In contrast, the thermalization timescale will be $O(L)$ if the depolarizing channels are only applied at the boundary. Mapping this situation to the spin model, all triangle weights in the bulk will be the same as the $p = 0$ unitary-only case where only vertical domain walls are allowed. To reach thermalization such that spins deep in the bulk are id , domain walls should look like Fig. 4(a). The timescale should be at least $O(L)$ to allow such configurations. In Fig. 4(b), we show the numerical results for a Clifford random circuit with boundary-only trace channels always applied ($p = 1$). The peak value clearly obeys a volume law [Fig. 4(c)].

The case of boundary-only depolarization may be related to the entanglement dynamics of a contiguous subsystem of a closed system evolving under random unitaries; this subsystem is coupled to its “environment” (the complement) through its boundary. [39] found that the bipartite operator entanglement of such a subsystem exhibits a volume law peak during the dynamics, consistent with our analysis and numerics.

Acknowledgements: We thank Tarun Grover, Yaodong Li, and Beni Yoshida for helpful discussions. This work was supported by Perimeter Institute, NSERC, and Compute Canada. Research at Perimeter Institute is supported in part by the Government of Canada through the Department of Innovation, Science and Economic De-

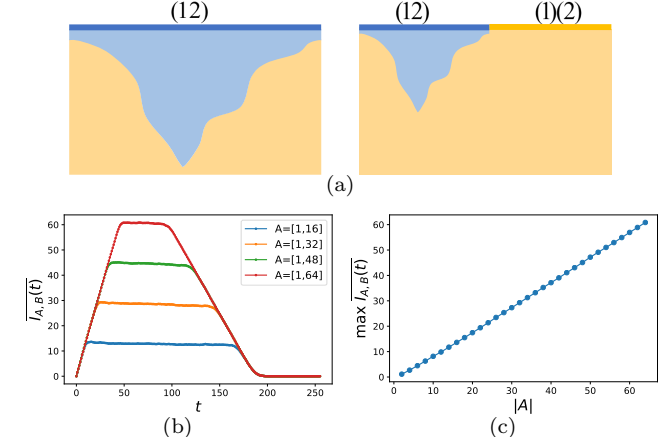


FIG. 4. Analysis and numerics for a setup with depolarizing channels only at the system boundary. (a) Domain wall configurations of the corresponding spin model. (b) Dynamics of the mutual information for various $|A|$ in the Clifford version. (c) Linear regression between the peak value and $|A|$. $L = 128$ in simulations above.

velopment and by the Province of Ontario through the Ministry of Colleges and Universities.

- [1] E.B. Davies and E.W. Davies, *Quantum Theory of Open Systems* (Academic Press, 1976).
- [2] Goran Lindblad, “On the generators of quantum dynamical semigroups,” *Communications in Mathematical Physics* **48**, 119–130 (1976).
- [3] Howard Carmichael, “An Open Systems Approach to Quantum Optics,” *Lecture Notes in Physics Monographs* **18** (1993).
- [4] Heinz-Peter Breuer, Francesco Petruccione, *et al.*, *The theory of open quantum systems* (Oxford University Press on Demand, 2002).
- [5] Robert Alicki and Karl Lendi, *Quantum dynamical semigroups and applications*, Vol. 717 (Springer, 2007).
- [6] Angel Rivas and Susana F Huelga, *Open quantum systems*, Vol. 10 (Springer, 2012).
- [7] John Preskill, “Quantum Computing in the NISQ era and beyond,” *Quantum* **2**, 79 (2018).
- [8] Guifré Vidal, “Efficient classical simulation of slightly en-

tangled quantum computations,” *Phys. Rev. Lett.* **91**, 147902 (2003).

[9] Kyungjoo Noh, Liang Jiang, and Bill Fefferman, “Efficient classical simulation of noisy random quantum circuits in one dimension,” *Quantum* **4**, 318 (2020).

[10] Yiqing Zhou, E. Miles Stoudenmire, and Xavier Waintal, “What limits the simulation of quantum computers?” *Phys. Rev. X* **10**, 041038 (2020).

[11] F. Verstraete, J. J. García-Ripoll, and J. I. Cirac, “Matrix product density operators: Simulation of finite-temperature and dissipative systems,” *Phys. Rev. Lett.* **93**, 207204 (2004).

[12] Michael Zwolak and Guifré Vidal, “Mixed-state dynamics in one-dimensional quantum lattice systems: A time-dependent superoperator renormalization algorithm,” *Phys. Rev. Lett.* **93**, 207205 (2004).

[13] Adam Nahum, Jonathan Ruhman, Sagar Vijay, and Jeongwan Haah, “Quantum entanglement growth under random unitary dynamics,” *Phys. Rev. X* **7**, 031016 (2017).

[14] Tianci Zhou and Adam Nahum, “Emergent statistical mechanics of entanglement in random unitary circuits,” *Phys. Rev. B* **99**, 174205 (2019).

[15] Amos Chan, Andrea De Luca, and J. T. Chalker, “Spectral statistics in spatially extended chaotic quantum many-body systems,” *Phys. Rev. Lett.* **121**, 060601 (2018).

[16] C. W. von Keyserlingk, Tibor Rakovszky, Frank Pollmann, and S. L. Sondhi, “Operator hydrodynamics, otocs, and entanglement growth in systems without conservation laws,” *Phys. Rev. X* **8**, 021013 (2018).

[17] Adam Nahum, Sagar Vijay, and Jeongwan Haah, “Operator spreading in random unitary circuits,” *Phys. Rev. X* **8**, 021014 (2018).

[18] Brian Skinner, Jonathan Ruhman, and Adam Nahum, “Measurement-induced phase transitions in the dynamics of entanglement,” *Phys. Rev. X* **9**, 031009 (2019).

[19] Yaodong Li, Xiao Chen, and Matthew P. A. Fisher, “Quantum zeno effect and the many-body entanglement transition,” *Phys. Rev. B* **98**, 205136 (2018).

[20] Amos Chan, Rahul M. Nandkishore, Michael Pretko, and Graeme Smith, “Unitary-projective entanglement dynamics,” *Phys. Rev. B* **99**, 224307 (2019).

[21] Lucas Sá, Pedro Ribeiro, Tankut Can, and Tomaž Prosen, “Spectral transitions and universal steady states in random kraus maps and circuits,” *Phys. Rev. B* **102**, 134310 (2020).

[22] Lucas Sá, Pedro Ribeiro, and Tomaž Prosen, “Integrable nonunitary open quantum circuits,” *Phys. Rev. B* **103**, 115132 (2021).

[23] Yaodong Li and Matthew Fisher, “Robust decoding in monitored dynamics of open quantum systems with Z_2 symmetry,” arXiv preprint arXiv:2108.04274 (2021).

[24] Zack Weinstein, Yimu Bao, and Ehud Altman, “Measurement-induced power law negativity in an open monitored quantum circuit,” arXiv preprint arXiv:2202.12905 (2022).

[25] Supplemental Material.

[26] G. Vidal and R. F. Werner, “Computable measure of entanglement,” *Phys. Rev. A* **65**, 032314 (2002).

[27] Jayendra N Bandyopadhyay and Arul Lakshminarayanan, “Entangling power of quantum chaotic evolutions via operator entanglement,” arXiv preprint quant-ph/0504052 (2005).

[28] Yimu Bao, Soonwon Choi, and Ehud Altman, “Theory of the phase transition in random unitary circuits with measurements,” *Phys. Rev. B* **101**, 104301 (2020).

[29] Chao-Ming Jian, Yi-Zhuang You, Romain Vasseur, and Andreas W. W. Ludwig, “Measurement-induced criticality in random quantum circuits,” *Phys. Rev. B* **101**, 104302 (2020).

[30] This expression is not valid if $d = 2$, since d is not very large. In this case, we can replace $\frac{1}{d}$ with the exact vertical domain wall contribution $\frac{d}{d^2+1}$ hence $\log \frac{d}{2}$ by $\log \frac{d^2+1}{2d}$.

[31] Using Eq. (12) instead of Eq. (11), we can get another timescale $t^{*'} = t^* + O(\frac{1}{L})$ which equals t^* in the thermodynamics limit.

[32] Sergey Bravyi, “Upper bounds on entangling rates of bipartite hamiltonians,” *Phys. Rev. A* **76**, 052319 (2007).

[33] Michaël Mariën, Koenraad MR Audenaert, Karel Van Acoleyen, and Frank Verstraete, “Entanglement rates and the stability of the area law for the entanglement entropy,” *Communications in Mathematical Physics* **346**, 35–73 (2016).

[34] Yadin Y. Goldschmidt, “Phase diagram of the potts model in an applied field,” *Phys. Rev. B* **24**, 1374–1383 (1981).

[35] Shan-Ho Tsai and D.P. Landau, “Phase diagram of a two-dimensional large-q potts model in an external field,” *Computer Physics Communications* **180**, 485–487 (2009), special issue based on the Conference on Computational Physics 2008.

[36] Daniel Gottesman, *Stabilizer codes and quantum error correction* (California Institute of Technology, 1997).

[37] There are some subtle differences, see [25], but the area law still holds.

[38] Neither the mutual information nor the log-negativity is convex. However, for stabilizer states, we have a structure theorem [40] which implies log-negativity equals the squashed entanglement [41], the latter being a nice convex measure for quantum entanglement.

[39] Huajia Wang and Tianci Zhou, “Barrier from chaos: operator entanglement dynamics of the reduced density matrix,” *Journal of High Energy Physics* **2019**, 1–44 (2019).

[40] Sergey Bravyi, David Fattal, and Daniel Gottesman, “Ghz extraction yield for multipartite stabilizer states,” *Journal of Mathematical Physics* **47**, 062106 (2006).

[41] Robert R Tucci, “Entanglement of distillation and conditional mutual information,” arXiv preprint quant-ph/0202144 (2002).

Supplemental material for “Entanglement dynamics of random quantum channels”

Zhi Li,¹ Shengqi Sang,^{1,2} and Timothy H. Hsieh¹

¹*Perimeter Institute for Theoretical Physics, Waterloo, Ontario N2L 2Y5, Canada*

²*Department of Physics and Astronomy, University of Waterloo, Waterloo, Ontario N2L 3G1, Canada*

CONTENTS

I. Derivation of the statistical mechanics model	1
A. Correlation and entanglement measures	1
B. Bulk theory	2
C. Boundary conditions	4
II. A small incremental theorem	4
III. large d expansion	5
A. Triangle weights	5
B. Small t	6
C. Large t	8
D. Area Law	10
IV. Probabilistic trace setup	11
A. Statistical mechanics model	11
B. Triangle weights	12
C. Small Incremental	13
V. Clifford simulation	13
A. One dimension	14
B. Two dimension	14
VI. One qudit toy model	14
A. Random channel setup	15
B. Probabilistic trace setup	15
References	16

I. DERIVATION OF THE STATISTICAL MECHANICS MODEL

A. Correlation and entanglement measures

Besides the Rényi mutual information

$$I_n(A:B) = S_{n,A} + S_{n,B} - S_{n,AB} = \frac{1}{1-n} [\log \text{tr}_A(\text{tr}_B \rho)^n + \log \text{tr}_B(\text{tr}_A \rho)^n - \log \text{tr} \rho^n] \quad (1)$$

considered in the main text, we will also be interested in the operator entanglement entropy and the (logarithmic) negativity.

The operator entanglement entropy for a (pure or mixed) state is the entanglement entropy for a corresponding normalized operator state. More precisely, a density matrix ρ on a bipartite system AB can be regarded as a state $|\rho\rangle$ in $H_{AB} \otimes H_{AB}^*$, where H_{AB}^* is the dual space of H_{AB} . This state is in general not normalized:

$$\|\rho\|^2 = \langle \rho | \rho \rangle = \text{tr} \rho^2. \quad (2)$$

The bipartite operator entanglement entropy is then:

$$S_{n,A,B}^{op} = \frac{1}{1-n} \log \text{tr}_A \left(\text{tr}_B \frac{|\rho\rangle\langle\rho|}{\|\rho\|^2} \right)^n = \frac{1}{1-n} \{ \log \text{tr}_A [\text{tr}_B (|\rho\rangle\langle\rho|)]^n - \log(\text{tr}\rho^2)^n \}. \quad (3)$$

The operator entanglement entropy measures the complexity to represent the density matrix as a matrix product operator (MPO), similar to the usual entanglement entropy measuring the complexity to represent the wave-function as a matrix product state (MPS). Like mutual information, it also measures both classical and quantum correlations.

The entanglement negativity is a useful quantity to measure the quantum entanglement for a bipartite system. The logarithmic negativity is defined as:

$$N_{A,B} = \log \|\rho^{\Gamma_A}\|_1, \quad (4)$$

where ρ^{Γ_A} is the partial transpose on B , $\|\cdot\|_1$ is the trace norm—sum of all singular values. Its Rényi generalization is defined as:

$$N_{n,A,B} = -\log \frac{\|\rho^{\Gamma_A}\|_n}{\text{tr}\rho^n} = -\log \text{tr} [(\rho^{\Gamma_A})^n] + \log \text{tr}\rho^n, \quad (5)$$

where $\|\cdot\|_1$ is the L^n norm. The second equation holds if n is an even integer.

We will be interested in the averaged quantity over trajectories ρ_t :

$$\bar{\mathcal{M}}(\rho_t) = \mathbb{E} [\mathcal{M}(\rho_t)], \quad (6)$$

where \mathbb{E} is the expectation value by averaging over circuit realizations and \mathcal{M} is $I_{n,A,B}$ or $S_{n,A,B}^{op}$ or $N_{n,A,B}$.

B. Bulk theory

To evaluate the logarithms appeared in Eqs. (1), (3) and (5), we use the replica trick:

$$\mathbb{E} \log X = \mathbb{E} \frac{\partial}{\partial \alpha} X^\alpha \Big|_{\alpha=0} = \frac{\partial}{\partial \alpha} \mathbb{E} X^\alpha \Big|_{\alpha=0} = \frac{\partial}{\partial \alpha} \log \mathbb{E} X^\alpha \Big|_{\alpha=0}. \quad (7)$$

Representing each ρ (and $|\rho\rangle$) as a 2-layer circuit (one layer for U and one layer for U^\dagger), traces evolved in Eqs. (1), (3) and (5) can be visualized as multi-layer circuits. Taking the replica trick into consideration, we need to work out the traces for generic number of layers. In the following, $2Q$ is the number of layers evolved; $Q = n\alpha$ for Eqs. (1) and (5); $Q = 2n\alpha$ for Eq. (3).

The random channel above adjacent qudits can be expressed as:

$$\Phi(\rho) = (1-p)\Phi_U(\rho) + p\Phi_T(\rho) = (1-p)U\rho U^\dagger + \frac{p\text{tr}(\rho)}{d^2}\mathbb{I}, \quad (8)$$

where Φ_U is the random unitary channel and Φ_T is the trace channel. Therefore,

$$\mathbb{E} (\Phi^{\otimes Q}) = \mathbb{E} [(1-p)\Phi_U + p\Phi_T]^{\otimes Q} = \sum_{k=1}^Q \sum_{i_1, \dots, i_k} (1-p)^{Q-k} p^k \mathbb{E} (\Phi_U \otimes \dots \otimes \Phi_T \otimes \dots \otimes \dots). \quad (9)$$

Here $\{i_1, \dots, i_k\}$ are the positions where Φ_T appears in $\Phi_U \otimes \dots \otimes \Phi_T \otimes \dots \otimes \dots$.

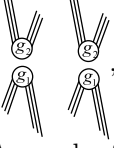
The only randomness here is the Haar randomness for the unitaries. We will make use of the following identity for Haar average of m pairs of U and U^\dagger :

$$\mathbb{E} (\Phi_U^{\otimes m}) = \mathbb{E} \left(\begin{array}{c} \text{orange blocks} \\ \text{white blocks} \end{array} \right) = \sum_{g_1, g_2 \in S_m} W(g_1^{-1} g_2) \text{ (circuit diagram)} \quad (10)$$

Here the orange blocks are Haar random unitaries U (and U^\dagger); $W_m()$ is the Weingarten function (it also depends on d^2 but we omit it); S_m is the permutation group over m elements. Therefore,

$$\mathbb{E}(\Phi_U \otimes \cdots \otimes \Phi_T \cdots \otimes \cdots) = \sum_{g_1, g_2 \in S_{Q-k}} \frac{W_{Q-k}(g_1^{-1} g_2)}{d^{2k}} \left(\begin{array}{c} \text{Diagram with } g_1 \\ \text{Diagram with } g_2 \end{array} \right) \otimes \left(\begin{array}{c} \text{Diagram with } id \\ \text{Diagram with } id \end{array} \right). \quad (11)$$

In the above equation, $g_1, g_2 \in S_{Q-k}$ and $id \in S_k$ (we omit the order of the tensor product to make the notation

clear). Plugging it into Eq. (9), we see that each term in Eq. (9) will be of the form , with now $g_1, g_2 \in S_n$.

However, a term with g_1, g_2 may come from more than one k and $\{i_1, \dots, i_k\}$. Any subset of the common fixed points of g_1, g_2 could come from the Φ_T part in Eq. (9) (equivalently, the id part in Eq. (11)). The coefficient before the g_1, g_2 term should be:

$$\sum_{i=0}^{n_{g_1, g_2}} \binom{n_{g_1, g_2}}{i} (1-p)^{Q-i} p^i \frac{W_{Q-i}(g_1^{-1} g_2)}{d^{2i}}. \quad (12)$$

Here n_{g_1, g_2} is the number of common fixed points of g_1 and g_2 . Combinatorial numbers appear because we need to pick up i elements from these fixed points and assume they come from the Φ_T part and other $Q-i$ legs come from the Φ_U part. Therefore:

$$\begin{aligned} \mathbb{E}(\Phi^{\otimes Q}) &= \sum_{g_1, g_2 \in S_Q} \frac{(1-p)^{Q-n_{g_1, g_2}}}{d^{2Q}} \sum_{i=0}^{n_{g_1, g_2}} \binom{n_{g_1, g_2}}{i} (1-p)^{n_{g_1, g_2}-i} p^i d^{2(Q-i)} W_{Q-i}(g_1^{-1} g_2) \left(\begin{array}{c} \text{Diagram with } g_1 \\ \text{Diagram with } g_2 \end{array} \right) \otimes \left(\begin{array}{c} \text{Diagram with } id \\ \text{Diagram with } id \end{array} \right) \\ &\stackrel{\text{def}}{=} \sum_{g_1, g_2 \in S_Q} \frac{(1-p)^{Q-n_{g_1, g_2}}}{d^{2Q}} V_Q(g_1, g_2) \left(\begin{array}{c} \text{Diagram with } g_1 \\ \text{Diagram with } g_2 \end{array} \right). \end{aligned} \quad (13)$$

Together with the cross-layer contractions

$$\left(\begin{array}{c} \text{Diagram with } g_2 \\ \text{Diagram with } g_1 \end{array} \right) = d^{Q-|g_1^{-1} g_2|}, \quad (14)$$

(here $|g|$ is the distance between g and id in S_Q , which equals the minimal number of transpositions in g ; equivalently $Q-|g|$ is the number of cycles in the cycle decomposition of g), we arrive at a statistical model on the honeycomb lattice. On each lattice, there is a S_Q spin g ; the statistical weight for a spin configuration $\{g\}$ is given by:

$$\prod_v (1-p)^{Q-n_{g_1, g_2}} V_Q(g_1, g_2) \prod_h d^{-|g_1^{-1} g_2|}. \quad (15)$$

Here v means vertical bonds and h means horizontal (zigzag) bonds. $V_Q(g_1, g_2)$ is Eq. (13) multiplied by d^{2Q} . The $\frac{1}{d^{2Q}}$ factor in Eq. (13) is exactly cancelled by d^Q factors in Eq. (14) since each vertical bonds corresponds to two horizontal bonds.

The triangle weights are obtained by integrating out spins at the top of each vertical bonds. We have:

$$\left(\begin{array}{c} b \\ \diagdown \\ a \\ \diagup \\ c \end{array} \right) = \sum_{\tau \in S_Q} \left(\begin{array}{c} b \\ \diagdown \\ \tau \\ \diagup \\ a \\ \diagdown \\ c \end{array} \right) = (1-p)^{Q-n_a} K_p(a, b, c) \quad (16)$$

where n_a is the number of fix points in a and

$$K_p(a, b, c) = \sum_{\tau \in S_Q} d^{-|\tau^{-1}b| - |\tau^{-1}c|} (1-p)^{n_a - n_{\tau, a}} V_Q(\tau, a). \quad (17)$$

C. Boundary conditions

The bottom boundary corresponds to the initial state, which we choose to be a product pure state. Under the Haar average Eq. (10), we should attach a state $|\psi\rangle$ to the open ends at the bottom, which effectively leaves the permutations alone (basically because $\langle\psi|\psi\rangle = 1$). Therefore the boundaries at the bottom are always free (on the contrary if the initial state is the maximally mixed state, the bottom boundary should obey a fixed boundary condition where all spins are fixed to id).

On the top boundary, the traces are the ways to contract the layers, which amounts to fixed boundary conditions for the spins. Here, we list the boundary conditions for each quantity.

For $I_n(A:B)$, if the replica number $\alpha = 1$, then the first term amounts to fixing spins above B region to $a = id_n$ and fixing spins above A region to $b = (1, 2, \dots, n)$; the second term is similar; the third term amounts to fixing spins to b everywhere. With $\alpha \geq 2$, we need to repeat the above pattern α times, so $a = id_Q$, $b = (1, 2, \dots, n)(n+1, n+2, \dots, 2n) \dots (\dots, Q)$. At the end, Eq. (1) becomes

$$\overline{I_n(A:B)} = \frac{n}{1-n} \frac{\partial}{\partial Q} (\log \mathcal{Z}_{ba} + \log \mathcal{Z}_{ab} - \log \mathcal{Z}_{bb}). \quad (18)$$

where the subscripts indicate different boundary conditions in the partition function \mathcal{Z} .

For $S_{n,A}^{op}$ and $\alpha = 1$, the first term amounts to fixing spins above A region to $c = (2, 3)(4, 5) \dots (2n, 1)$ and fixing spins above B region to $d = (1, 2)(3, 4) \dots (2n-1, 2n)$, the second term amounts to fixing spins to d everywhere. With $\alpha \geq 2$, c becomes $(2, 3)(4, 5) \dots (2n, 1)(2n+2, 2n+3) \dots (4n, 2n+1) \dots (Q, Q-2n+1)$, d becomes $(1, 2)(3, 4) \dots (Q-1, Q)$. Eq. (3) becomes

$$\overline{S_{n,A}^{op}} = \frac{2n}{1-n} \frac{\partial}{\partial Q} (\log \mathcal{Z}_{cd} - \log \mathcal{Z}_{dd}). \quad (19)$$

For $N_{n,A,B}$ and $\alpha = 1$, the first term amounts to fixing spins above A to $e = (n, n-1 \dots, 1)$ and fixing spins above B to $b = (1, 2, \dots, n)$, the second term amounts to fixing spins to b everywhere. With $\alpha \geq 2$, e becomes $(n, n-1 \dots, 1)(2n, 2n-1 \dots, n+1) \dots (Q, Q-1 \dots, Q-n+1)$, b is the same as in $I_n(A:B)$. Eq. (3) becomes

$$\overline{N_{n,A,B}} = \frac{n\partial}{\partial Q} (\log \mathcal{Z}_{eb} - \log \mathcal{Z}_{bb}). \quad (20)$$

If we focus on Rényi-2 $I(A:B)$ and S^{op} , then $n = 2$, $b = d = (1, 2)(3, 4) \dots (Q-1, Q)$, $c = (1, 4)(2, 3)(5, 8)(6, 7) \dots$. As a side note, we have the following formula for the Rényi-2 entropy of the whole system:

$$\overline{S_2} = -2 \frac{\partial}{\partial Q} \log \mathcal{Z}_{bb}. \quad (21)$$

II. A SMALL INCREMENTAL THEOREM

We prove that mutual information grows at most linearly in time. Consider any bipartite system AB , consider $I(A:B)$. There are two types of channels:

- For a channel Φ acting inside A or B , $I(\Phi(A):\Phi(B)) \leq I(A:B)$ according to the data processing inequality/monotonicity of mutual information.
- For a channel Φ acting on the boundary between A and B , $I(A:B)$ can only increase a constant. Indeed, denote the qubits at the boundary as a and b ($a \in A$ and $b \in B$), then after the action:

$$\begin{aligned} I'(A:B) &= S'(A) + S'(B) - S'(AB) \\ &\leq S'(A-a) + S'(a) + S'(B-b) + S'(b) - S'(AB) \\ &\leq S(A-a) + S'(a) + S(B-b) + S'(b) - S(AB) \\ &\leq S(A) + S(a) + S'(a) + S(B) + S(b) + S'(b) - S(AB) \\ &= S(a) + S'(a) + S(b) + S'(b) + I(A:B). \end{aligned} \quad (22)$$

Here the first and third inequalities are due to the triangle inequality of entropy; the second inequality is because $S(\Phi(AB)) \geq S(AB)$ (since Φ is unital) and $S'(A-a) = S(A-a)$ since Φ does not touch $A-a$.

Since there is only one boundary unitary in each time layer, $I(A:B)$ grows at most linearly. The maximal slope is $O(\log d)$.

III. LARGE d EXPANSION

Following Ref. [1], we visualize the spin configurations in terms of domain wall configurations. The number of domain walls across the edge $a-b$ is equal to $|a^{-1}b|$. We will work in the large d limit and only keep terms with leading order in $\frac{1}{d}$ in all triangle weights.

A. Triangle weights

First of all [2],

$$d^{2(Q-i)} W_{Q-i}(g) = O\left(\frac{\text{Moeb}(g)}{d^{2|g|}}\right) + O\left(\frac{1}{d^{2|g|+4}}\right). \quad (23)$$

Importantly, the leading order coefficient $\text{Moeb}(g)$ only depends on the nontrivial part of g so it does not depend on i which tells us which permutation group g lives in. Therefore, to the leading order,

$$V_Q(g_1, g_2) = \sum_{i=0}^{n_{g_1, g_2}} \binom{n_{g_1, g_2}}{i} (1-p)^{n_{g_1, g_2}-i} p^i \frac{\text{Moeb}(g_1^{-1}g_2)}{d^{2|g_1^{-1}g_2|}} = \frac{\text{Moeb}(g_1^{-1}g_2)}{d^{2|g_1^{-1}g_2|}}, \quad (24)$$

$$K_p(a, b, c) = \sum_{\tau \in S_Q} (1-p)^{n_a - n_{\tau, a}} \text{Moeb}(\tau^{-1}a) d^{-|\tau^{-1}b| - |\tau^{-1}c| - 2|\tau^{-1}a|}. \quad (25)$$

According to the triangle inequality,

$$|\tau^{-1}b| + |\tau^{-1}c| + 2|\tau^{-1}a| \geq |a^{-1}b| + |a^{-1}c|, \quad (26)$$

where equality holds if and only if two “parallel” conditions are satisfied:

$$|\tau^{-1}b| + |\tau^{-1}a| = |a^{-1}b|, \quad \text{and} \quad |\tau^{-1}c| + |\tau^{-1}a| = |a^{-1}c|. \quad (27)$$

Hence to the leading order,

$$K_p(a, b, c) = d^{-|a^{-1}b| - |a^{-1}c|} \sum'_{\tau \in S_Q} (1-p)^{n_a - n_{\tau, a}} \text{Moeb}(\tau^{-1}a), \quad (28)$$

where \sum' means summation over all τ satisfying Eq. (27).

For us, the relevant graphs are of the following form:



We denote the number of $\backslash, /, \diagup, \diagdown$ as x, y, z . These $(x+y+z)$ lines are commuting domain walls: each domain wall is a transposition and these transpositions have no common elements thus commuting to each other. An example satisfying this graph is the following:

$$\begin{aligned} b^{-1}a &= (1, 2) \cdots (2z-1, 2z)(2z+1, 2z+2) \cdots (2x+2z-1, 2x+2z), \\ c^{-1}a &= (1, 2) \cdots (2z-1, 2z)(2x+2z+1, 2x+2z+2) \cdots (2x+2y+2z-1, 2x+2y+2z). \end{aligned} \quad (30)$$

Then τ has 2^z choices: $\tau^{-1}a$ is the product of some involutions choosing from $(1, 2), (3, 4), \dots, (2z-1, 2z)$. Within such restriction,

$$\text{Moeb}(\tau^{-1}a) = (-1)^{|\tau^{-1}a|}. \quad (31)$$

Moreover, notice that $n_a - n_{\tau,a} = n_a - n_{\tau^{-1}a,a}$ is the number of points invariant under a but change under $\tau^{-1}a$, which is the number of fixed points of a restricting on the non-fixed part of $\tau^{-1}a$. For example, if $\tau^{-1}a = (1, 2)(3)(4) \in S_4$, then $n_a - n_{\tau,a} = n(a|_{\{1,2\}})$ which is just $\delta_{a(1),1} + \delta_{a(2),2}$. Hence, in the example Eq. (30),

$$K_p(a, b, c) = \frac{1}{d^{x+y+2z}} \prod_{i=1}^z \left[1 - (1-p)^{n(a|_{\{2i-1, 2i\}})} \right]. \quad (32)$$

The key message here is: at the leading order of $\frac{1}{d}$, commuting domain walls are effectively independent of each other. Each \backslash or $/$ contributes $\frac{1}{d}$; each \sim contributes $\frac{1-(1-p)^*}{d^2}$. As a sanity check, the contribution of \sim vanishes if $p = 0$, which is known in the treatment of unitary-only circuits.

B. Small t

It is easiest to consider S^{op} Eq. (19) first. For the second term \mathcal{Z}_{dd} , there is only one configuration with lowest order of $\frac{1}{d}$: all spins should be equal to d , see Fig. 1(a). The number of fixed points $n_d = 0$, the number of triangles is $\frac{Lt}{2}$, so the partition function is:

$$\mathcal{Z}_{dd} \approx (1-p)^{\frac{QLt}{2}}. \quad (33)$$

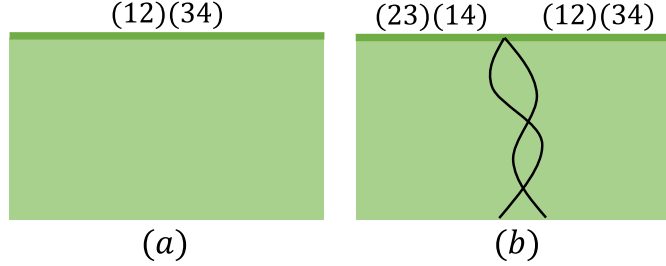


FIG. 1. Domain wall configuration for S^{op} at small t ($Q = 4$ for illustration). The thick line on the upper boundary indicates the fixed boundary condition. In (a), all spins are $d = (12)(34)$. In (b), spins can be different, hence the domain wall. In this case all spins have the same number of fixed points ($=0$), so they are colored with the same color.

For the first term \mathcal{Z}_{cd} , since $c^{-1}d = (1, 3)(2, 4) \cdots$, we know there must be $\frac{Q}{2}$ commuting domain walls starting from the intersection point. To get the lowest order in $\frac{1}{d}$, the domain walls need to propagate vertically to the bottom (because horizontal domain walls cost some extra factors of $\frac{1}{d^2}$), see Fig. 1(b). Therefore each domain wall contributes a weight $\frac{1}{d^t}$. Each domain wall also has an entropic contribution 2^t : it can go left or right at each step. Moreover, it is easy to check that all spins have no fixed points no matter how these domain walls locate, hence each triangle also contributes a $(1-p)^Q$. Therefore,

$$\mathcal{Z}_{cd} \approx (1-p)^{\frac{QLt}{2}} \left(\frac{2^t}{d^t} \right)^{\frac{Q}{2}}. \quad (34)$$

The Rényi-2 entropy of the whole system and the operator entanglement entropy are given by:

$$\overline{S_2}(t) = -2 \frac{\partial}{\partial Q} \log \mathcal{Z}_{dd} \approx (L \log \frac{1}{1-p})t, \quad (35)$$

$$\overline{S_{2,A}^{op}}(t) = -4 \frac{\partial}{\partial Q} (\log \mathcal{Z}_{cd} - \log \mathcal{Z}_{dd}) \approx (2 \log \frac{d}{2})t. \quad (36)$$

The last expression is not valid if $d = 2$, since d is not very large. In this case, we can replace $\frac{1}{d}$ with the exact vertical domain wall contribution $\frac{d}{d^2+1}$:

$$\overline{S_{2,A}^{op}}(t) \approx (2 \log \frac{d^2+1}{2d})t. \quad (37)$$

Now let us consider $I_{2,A,B}$ Eq. (18). The third term \mathcal{Z}_{bb} has been calculated in Eq. (33) since $b = d = (1, 2)(3, 4) \cdots (Q-1, Q)$.

For the first term \mathcal{Z}_{ba} , there must be $\frac{Q}{2}$ commuting domain walls starting from the intersection point propagating vertically to the bottom. However, this time spins could have different numbers of fixed points. For example, in the middle figure Fig. 2 we show a configuration for $Q = 2$. Spins on the right side of the domain wall are equal to id , hence they contribute 1 instead of $(1-p)^2$. Luckily, if a configuration only contains $\frac{Q}{2}$ commuting domain walls, one

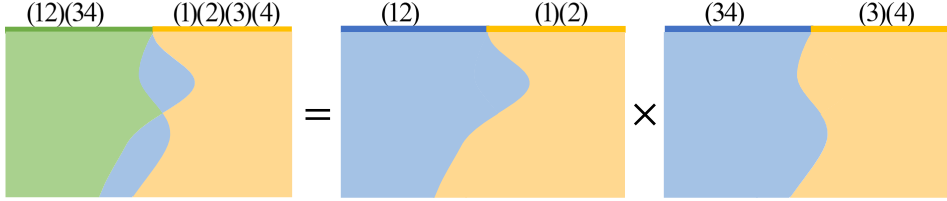


FIG. 2. Domain wall configuration for I_2 at small t . Blue spins are (12) or (34) ; green spins are $(12)(34)$; yellow spins are id . Two regions are separated by a domain wall. The first figure shows a configuration with $Q = 4$; it has two commuting domain walls. It can be decomposed as a product of two single domain wall configurations.

can decompose the configuration as a superposition of $\frac{Q}{2}$ configurations with only one type of domain wall, and the number of unfixed points exactly equals the summation of unfixed points for each:

$$Q - n_a = \sum_i^{Q/2} (2 - \tilde{n}_{a_i}). \quad (38)$$

Here, we decompose $a \in S_Q$ as the product of a_i where $a_i \in S_2^{(i)} = \{id, (2i+1, 2i+2)\}$. \tilde{n}_{a_i} is the number of fixed points of a_i defined in that $S_2^{(i)}$ (so $\tilde{n}_{id} = 2$). See Fig. 2 for illustration. Since commuting domain walls behaves independently to the leading order, we have:

$$\mathcal{Z}_{ba}(Q) \approx [\mathcal{Z}_{ba}(Q=2)]^{Q/2}. \quad (39)$$

Therefore the calculation reduces to the case with only one domain wall.

To calculate the entropic contribution, let us represent a domain wall by a vector $x = (x_1, x_2, \dots, x_t)$, where $x_i = \pm 1$ if the i -th step turns right or left (from our perspective). Then the number of $(1-p)^2$ factors equals:

$$\frac{Lt}{4} - \frac{x_1}{2} + \frac{x_1 + x_2}{2} + \dots + \frac{x_1 + x_2 + \dots + x_t}{2} = \frac{Lt}{4} + \sum_{i=1}^t \frac{(t+1-i)x_i}{2}. \quad (40)$$

Therefore,

$$\mathcal{Z}_{ab}(Q=2) = \mathcal{Z}_{ba}(Q=2) \approx \frac{1}{d^t} \sum_x (1-p)^{\frac{Lt}{2} - \sum_{i=1}^t (t+1-i)x_i} = \frac{2^t}{d^t} (1-p)^{\frac{Lt}{2}} \prod_{i=1}^t \frac{(1-p)^{-i} + (1-p)^i}{2}. \quad (41)$$

Finally, the Rényi-2 mutual information is given by:

$$\overline{I_2(A:B)} \approx (2 \log \frac{d}{2})t - 2 \sum_{i=1}^t \log \frac{(1-p)^{-i} + (1-p)^i}{2}. \quad (42)$$

We note that, the extra term in Eq. (42) compared to Eq. (36) does not change the initial slope¹.

¹ This can be understood by noticing that the difference at t and $t-1$ is $2 \log \frac{(1-p)^{-t} + (1-p)^t}{2}$, which converges to 0 as $t \rightarrow 0$. A more serious treatment can be done by using q-series.

C. Large t

When t is large enough, we expect the system to be maximally mixed:

$$\rho(t \rightarrow \infty) = \frac{\mathbb{I}}{d^L}. \quad (43)$$

Various partition functions in Eqs. (18) to (20), which corresponding to various traces in Eqs. (1), (3) and (5), can be easily calculated in this limit. For example,

$$\mathcal{Z}_{ba} = (\text{tr}_A (\text{tr}_B \frac{\mathbb{I}}{d^L})^2)^\alpha = \frac{1}{d^{|A|\alpha}} = \frac{1}{d^{|A|Q/2}}. \quad (44)$$

Similarly,

$$\mathcal{Z}_{ab} = \frac{1}{d^{|B|Q/2}} \quad \mathcal{Z}_{bb} = \mathcal{Z}_{dd} = \mathcal{Z}_{cd} = \frac{1}{d^{LQ/2}}. \quad (45)$$

Therefore, Eqs. (18) to (20) vanish as expected.

In this subsection, we show that the summing over horizontal domain wall configurations can be exactly carried out in the statistical mechanics model, and the results match with the limits at Eq. (43). We will eventually calculate the partition functions for arbitrary layer numbers. However, the logic in Eqs. (38) and (39) still applies here, so we only need to focus on $Q = 2$.

To be precise, we will sum over configurations satisfying the following conditions:

- the number of domain walls is minimal (no “bubbles”);
- domain walls are *horizontally directed*: projecting horizontally, the domain wall can never overlap.

The reason to restrict the configurations is to keep the exponent of $\frac{1}{d}$ minimal, since each horizontal segment will contribute a $\frac{1}{d}$ factor (also see below). In Fig. 3, we illustrate these two conditions for terms for $Q = 2$.

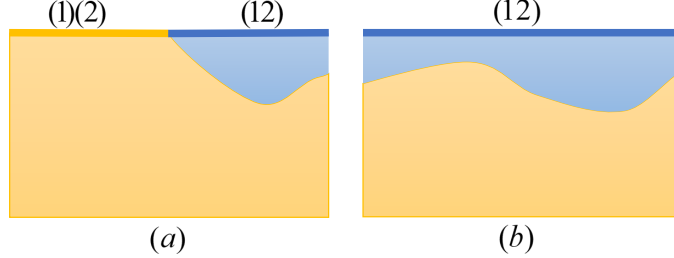


FIG. 3. Domain wall configuration at large t for $Q = 2$. Blue spins are (12) and yellow spins are $id = (1)(2)$. The domain walls are horizontally directed.

The relevant graphically rules are summarized as follows:

- vertical-horizontal segment \backslash contributes $\frac{1}{d}$ (boundary contribution);
- horizontal-horizontal segment \sim contributes $\frac{1-(1-p)^2}{d^2}$ (boundary contribution);
- each triangle above the domain wall contributes $(1-p)^2$ (area contribution).

Let us first consider the “hanging” configurations such that the distance between endpoints is n (the domain wall is necessarily vertical at the endpoints). Denote the summation of these configurations as u_n . As shown in Fig. 4, the domain wall can either go right at the first step, or firstly go down then return to the boundary at position k ($1 \leq k \leq n-1$) then go right one more step, or firstly go down then return for the first time at position n . Therefore:

$$u_n = \frac{1-(1-p)^2}{d^2} u_{n-1} + \sum_{k=1}^{n-1} (1-p)^{2k} \frac{1}{d} u_{k-1} \frac{1}{d} \frac{1-(1-p)^2}{d^2} u_{n-1-k} + (1-p)^{2n} \frac{1}{d} u_{n-1} \frac{1}{d}. \quad (46)$$

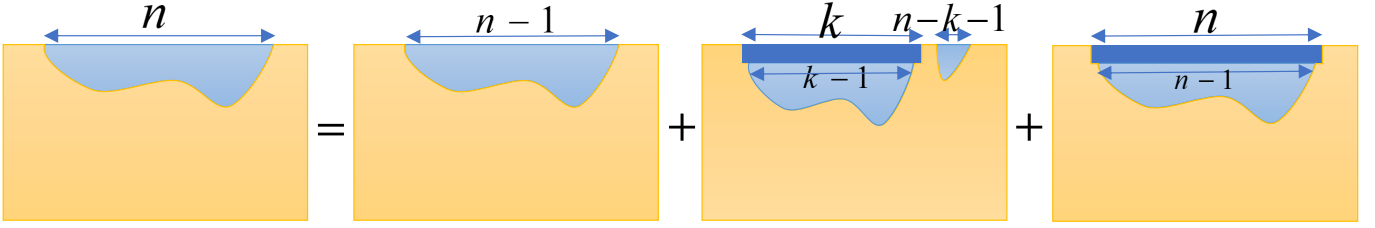


FIG. 4. Iteration relations used in the calculation. Each rectangular represents a summation of some configurations. Dark blue means those spins are guaranteed to be (12) — in other words, the domain wall is at least 1 step away from the upper boundary; light blue means the domain wall can sometimes attach to the upper boundary.

With this iteration relation and the initial condition $u_0 = 1$, one can easily verify that

$$u_n = \frac{1}{d^{2n}}. \quad (47)$$

To calculate \mathcal{Z}_{ba} , denote v_n to be the summation of configurations where domain walls' right endpoints are on the right boundary (n is the distance between the left endpoint and the right boundary). Due to the (left and right) boundary conditions, there are actually two types of v , depending on whether the total number of layers is even or odd. We use v and v' to distinguish them. Similarly to Eq. (46), we have:

$$v_n = \frac{1 - (1-p)^2}{d^2} v_{n-1} + \sum_{k=1}^{n-1} (1-p)^{2k} \frac{1}{d} u_{k-1} \frac{1}{d} \frac{1 - (1-p)^2}{d^2} v_{n-1-k} + (1-p)^{2n} \frac{1}{d} v'_n. \quad (48)$$

$$v'_n = \frac{1 - (1-p)^2}{d^2} v'_{n-1} + \sum_{k=1}^{n-1} (1-p)^{2k} \frac{1}{d} u_{k-1} \frac{1}{d} \frac{1 - (1-p)^2}{d^2} v'_{n-1-k} + (1-p)^{2n} \frac{1}{d} v_{n-1}. \quad (49)$$

With this iteration relation and the initial condition $v'_0 = 1$, one can verify that:

$$v_n = \frac{1}{d^{2n+1}}, \quad v'_n = \frac{1}{d^{2n}}. \quad (50)$$

(Less rigorously, one can regard this result as the limit of Eq. (46) by taking the right endpoint to the right boundary.) Therefore,

$$\mathcal{Z}_{ba} = \frac{1}{d^{|A|}}. \quad (51)$$

It is consistent with Eq. (44)

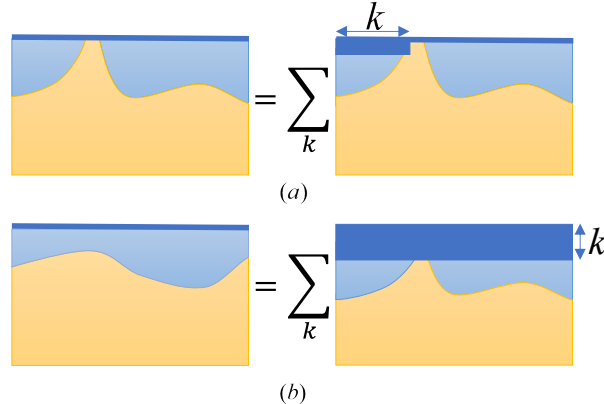


FIG. 5. Relations used to calculate \mathcal{Z}_{bb} . Blue spins are (12) and yellow spins are $id = (1)(2)$.

To calculate \mathcal{Z}_{bb} , denote w to be the summation of configurations where domain walls are attached to the upper boundary for at least one segment, see Fig. 5(a). By classifying the position of the first attachment point, we have:

$$w = \sum_{k=0}^{L/2} (1-p)^{2k} \frac{1}{d} v'_k \frac{1 - (1-p)^2}{d^2} v_{L/2-k-2} = \frac{1 - (1-p)^L}{d^L}. \quad (52)$$

Noticing Fig. 5(b), we have:

$$\mathcal{Z}_{bb} = \sum_{k=0}^{\infty} (1-p)^{kL} w = \frac{1}{d^L}. \quad (53)$$

Alternatively, one can regard this result as the limit $n \rightarrow L/2$ in Eq. (46) by taking both endpoints to the boundaries. The result is consistent with Eq. (45).

D. Area Law

The argument for area law works as follows: due to the at most linear growth, the mutual information $I(A:B)$ at time t^* can at most be $O(t^*)$. After t^* time scale, the system is trivialized and we anticipate that $I(A:B)$ is at most $O(1)$. Therefore, the maximal value for $I(A:B)$ can at most be $O(t^*)$. However, as shown in the main text, three terms $S(A)$, $S(B)$, $S(AB)$ appeared in $I(A:B)$ are all extensive: they are $O(L)$ at any time. Therefore, $I(A:B)|_{t>t^*} < O(1)$ requires a delicate cancellation. In the following, we argue that this cancellation is quite natural.

For simplicity we set $|A|=|B|=L/2$. We anticipate:

$$S(AB)(t) - S(AB)|_{t=\infty} = -L f_1(L, t), \quad (54)$$

$$S(A)(t) - S(A)|_{t=\infty} = -\frac{L}{2} f_2(L, t) + f_3(L, t). \quad (55)$$

Here, $f_i(L, t)$ are almost L independent; $f_3(L, t)$ are bounded by some $O(1)$ value if $t > O(t^*)$. The absence of extra term in the first equation is due to the translational invariance. The fact of $O(1)$ thermalization time scale means

$$f_i(L, t) \sim C_i e^{-t/t_i}, \quad (56)$$

where $C_i \in \mathbb{R}$ and $t_i \in \mathbb{R}_{>0}$ are some $O(1)$ value [$t_1 = O(t^*)$]. By the small incremental result and nonnegativity of mutual information, we know rigorously:

$$-O(1) < [f_1(L, t) - f_2(L, t)]L < C_3 t - O(1) \quad \text{for } t > O(t^*). \quad (57)$$

A feature of the function $g(t) = C_1 e^{-t/t_1} - C_2 e^{-t/t_2}$ is that it has at most one stationary point t_* in $[0, +\infty)$, which is by definition L independent (just ignore t_* if it does not exist). $g(t)$ monotonically approach 0 after t_* :

$$|g(t)| \leq |g(t_*)| \leq \max\{|g(t_*)|, |g(t^*)|\} \quad \text{for } t > O(t_*), \quad (58)$$

hence for $t > O(\max\{t_*, t^*\})$:

$$|g(t)|L \leq \max\{|g(t_*)|L, |g(t^*)|L\} \leq \max\{|C_3 t_* - O(1)|, |C_3 t^* - O(1)|, |O(1)|\} = O(1). \quad (59)$$

The last equation is because t_* and t^* are L -independent. Due to Eq. (56) it is natural to expect that $f_2(L, t) - f_1(L, t)$ satisfies similar property as Eq. (58), perhaps with some extra constant. Thus, $I(A:B) < O(1)$ for t larger than some L -independent value.

The area law can also be understood assuming horizontally directed domain walls are dominant when $t > O(t^*)$. Generalizing Eq. (52) to finite time, we have:

$$u_n(t) = \frac{p}{d^2} u_{n-1}(t) + \frac{p}{d^4} \sum_{k=1}^{n-1} (1-p)^k u_{k-1}(t-1) u_{n-1-k}(t) + \frac{(1-p)^n}{d^2} u_{n-1}(t-1). \quad (60)$$

Here, $u_n(t)$ is the summation of “hanging” configurations, under the restriction that the depth of the statistical mechanics system is t [with $t < \infty$, the domain wall can disappear at the lower boundary and then reappear at

a different point; to clarify, $u_n(t)$ is actually a decreasing function of t due to the decrease of domain wall length although there are more configurations at larger t]. The boundary conditions are:

$$u_{n \geq 0}(t=0) = d^2, \quad u_0(t \geq 1) = 1. \quad (61)$$

Although we do not have an analytical expression for $u_n(t)$, the following statement can be numerically checked for $t > O(t^*)$:

$$\frac{u_0(t)u_{L/2}(t)}{u_{L/4}(t)^2} < O(1), \quad (62)$$

and this implies the area law.

IV. PROBABILISTIC TRACE SETUP

In the probabilistic trace setup, ‘‘trace channels’’ are applied probabilistically. Different from the original depolarizing channel setup, here each quantum trajectory/circuit is realized by fixing the unitaries *as well as* the presence/non-presence of each trace channel. Individual $\rho(t)$ does not contain p . The parameter p appears only at the level of averaging over quantum trajectories.

A. Statistical mechanics model

This setup can be mapped to a statistical mechanics model similarly.

Since

$$\text{[Diagram of a blue block with a dashed line above it]} = \begin{cases} \frac{1}{d^2} \text{[Diagram of a blue block with a dashed line above it and a vertical line below it]}, & \text{with prob=}p \\ \text{[Diagram of an orange block with a dashed line above it and a vertical line below it]}, & \text{with prob=}1-p \text{ and } U \text{ random} \end{cases}, \quad (63)$$

we have:

$$\begin{aligned} \mathbb{E}_C \left(\text{[Diagram of a blue block with a dashed line above it and a vertical line below it]} \right) &= \frac{p}{d^{2Q}} \text{[Diagram of a blue block with a dashed line above it and a vertical line below it]} + (1-p) \mathbb{E}_U \left(\text{[Diagram of an orange block with a dashed line above it and a vertical line below it]} \right) \\ &= \frac{p}{d^{2Q}} \text{[Diagram of a blue block with a dashed line above it and a vertical line below it]} + (1-p) \sum_{g_1, g_2 \in S_{2n}} W_Q(g_1^{-1}g_2) \text{[Diagram of a blue block with a dashed line above it and a vertical line below it]} \text{[Diagram of an orange block with a dashed line above it and a vertical line below it]}. \end{aligned} \quad (64)$$

Here the orange blocks are Haar random unitaries U and U^\dagger ; we use dashed lines for trace because we may or may not apply it; $W_Q()$ is the Weingarten function.

Following similar calculations towards Eq. (15), we obtain the spin model on the honeycomb lattice with the following weights:

$$\prod_v \left[\frac{p}{d^{2Q}} \delta_{g_1} \delta_{g_2} + (1-p) W_Q(g_1^{-1}g_2) \right] \prod_h d^{Q-|g_1^{-1}g_2|}. \quad (65)$$

See comments around Eq. (15) for notations.

Then we integrate over the upper spins for each vertical bonds:

$$\begin{aligned}
 \text{Diagram: } & \text{A triangle with vertices } a, b, c. \\
 & = \sum_{\tau \in S_Q} \text{Diagram: } \begin{array}{c} b \\ \diagup \quad \diagdown \\ \tau \\ \diagdown \quad \diagup \\ a \end{array} \\
 & = \sum_{\tau \in S_Q} d^{-|\tau^{-1}b| - |\tau^{-1}c|} [p\delta_{\tau}\delta_a + (1-p)d^{2Q}W_Q(\tau^{-1}a)]. \\
 & = pd^{-|b|-|c|}\delta_a + (1-p)J_0(a, b, c).
 \end{aligned} \tag{66}$$

Here J_0 is exactly the triangle weight in the unitary-only case ($p = 0$):

$$J_0(a, b, c) = \sum_{\tau \in S_Q} d^{2Q-|\tau^{-1}b|-|\tau^{-1}c|} W(\tau^{-1}a). \tag{67}$$

B. Triangle weights

The triangle weights can be simply obtained using results for the $p = 0$ case. Some results are shown in Tab. I.

$J_p(a, b, c)$							
$a \neq id$	$1-p$	$\frac{1-p}{d}$	0	0	0	$\frac{1-p}{d^2}$	$\frac{1-p}{d^2}$
$a = id$	1	$\frac{1}{d}$	$\frac{p}{d^2}$	$\frac{p}{d^3}$	$\frac{p}{d^3}$	$\frac{1}{d^2}$	$\frac{1}{d^2}$
$p = 0$	1	$\frac{1}{d}$	0	0	0	$\frac{1}{d^2}$	$\frac{1}{d^2}$

TABLE I. Triangle weights J_p for the statistical model. Here a is the spin of the downward vertex.

We see that the physical effects of the depolarization are still similar as before:

- Polarization field. If $p > 0$, the bottom spins are more probable to be id , due to a relative weight of 1 versus $(1-p)$.
- Horizontal domain wall. If $p > 0$, domain walls can propagate horizontally. This is only possible when the bottom spin equals id , again with an extra penalty of $\frac{1}{d}$ and a factor (here it is p) to restore the light cone for $p = 0$.

Up to $O(\frac{1}{d})$, the triangle weights in Tab. I can be equivalently summarized as:

$$E = -\log d \sum_{\langle ij \rangle} (\delta_{\sigma_i \sigma_j} - 1) - \log \frac{1}{1-p} \sum_i (\delta_{\sigma_i} - 1), \tag{68}$$

which is the Q !-state Potts model with magnetic field on a (rotated) two-dimensional square lattice. For $Q = 2$ it goes back to the Ising model in the main text. Moreover, for $Q = 2$, if we define p' by

$$(1-p')^2 = 1-p, \tag{69}$$

then the weights have the same form as in the random channel set up Eq. (32) (in terms of p') to the order $O(\frac{1}{d^2})$. Therefore, two models should share very similar properties. In particular, the system thermalizes in a system-size-independent time, and the mutual information peak value obeys an area law.

However, if $Q > 2$, triangle weights no longer factorize as Eq. (32). This means interactions between replicas are no longer negligible. For example, denote $a = (1, 2)(3, 4)$, $b = (1, 2)$, then:

$$\begin{aligned}
 J_p(id, a, a) &= \frac{p}{d^4} \neq J_p(id, b, b)J_p(id, b, b) = \frac{p^2}{d^4} \\
 &\neq J_p(b, a, a)J_p(b, a, a) = 0.
 \end{aligned} \tag{70}$$

Another example is, the counterpart of Eq. (33) will be $(1-p)^{L^{t/2}}$, which is independent on Q .

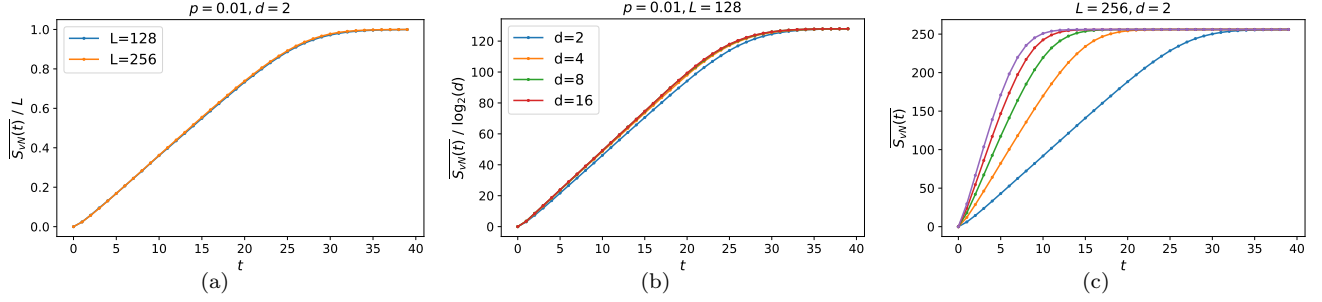


FIG. 6. Simulated state's von-Neumann entropy $S_{\text{vN}}(t)$ for various different (a) system size L , (b) onsite dimension d , and (c) decoherence frequency p .

C. Small Incremental

In this setting, we can also prove that the mutual information $I(A: B)$ grows at most linearly. There are three types of effects:

- For a trace channel, no matter acting inside A (or B) or on the boundary, $I(A: B)$ cannot increase, due to the monotonicity of mutual information.
- For a unitary acting inside A or B , $I(A: B)$ does not change.
- For a unitary acting on the boundary between A and B , $I(A: B)$ can only increase a constant:

$$\begin{aligned}
 I'(A: B) &= S'(A) + S'(B) - S'(AB) \\
 &\leq S'(A - a) + S'(a) + S'(B - b) + S'(b) - S'(AB) \\
 &= S(A - a) + S'(a) + S(B - b) + S'(b) - S(AB) \\
 &\leq S(A) + S(a) + S'(a) + S(B) + S(b) + S'(b) - S(AB) \\
 &= S(a) + S'(a) + S(b) + S'(b) + I(A: B).
 \end{aligned} \tag{71}$$

Here two inequalities are due to the triangle inequality.

Since there is only one boundary unitary in each time layer, $I(A: B)$ at most grows linearly.

V. CLIFFORD SIMULATION

Here we provide further numerical results of the Clifford circuits with the probabilistic trace setup. For all the numerical results shown below the initial state is always a product state $|0\rangle^{\otimes N}$, and the periodic boundary condition is always adapted.

First, we comment on some properties of stabilizer states.

- Stabilizer states (pure or mixed) always have flat entanglement spectra, so the Rényi entropy does not depend on the index n and equals the von Neumann value. The statement also holds for Rényi mutual information, operator entanglement entropy, and negativity².
- The entanglement structure of stabilizer states is very clear due to a structure theorem [3]. For stabilizer states, (1) operator entanglement entropy equals the mutual information, which counts the amount of both classical and quantum correlations; (2) log-negativity counts the quantum part of the correlations.

² Could up to a state-independent factor depending on the convention.

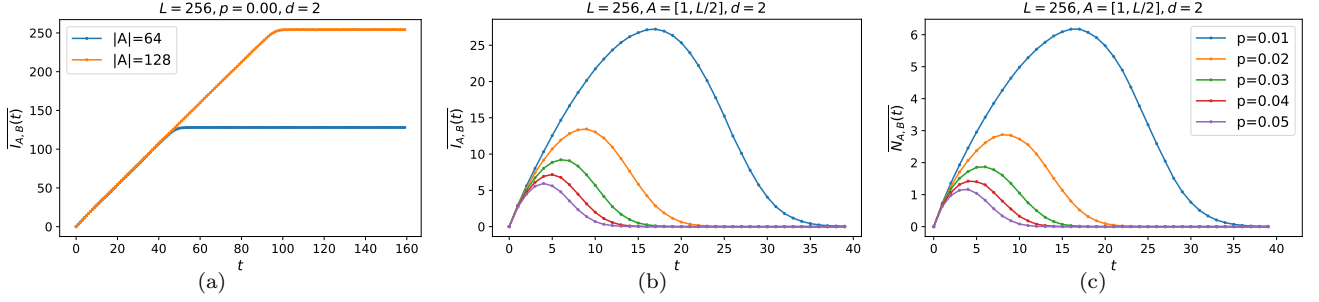


FIG. 7. Numerical results for entanglement measures between A and B , in a (1+1)D circuit. (a)(b) Mutual information for the $p = 0$ unitary-only case and for various nonzero p values. (c) Logarithmic entanglement negativity between A and B for various nonzero p values.

A. One dimension

Due to the extensive presence of trace channels, the coherence of the system will gradually lose with time. This effect can be detected by the whole system's total entropy S_{vN} , which also quantifies the correlation between the system and the environment. As shown in Fig. 6(a,b), the simulated $S_{\text{vN}}(t)$ grows and saturates to a volume law value in $O(1)$ time, and takes the form:

$$S_{\text{vN}}(t) \approx \frac{L}{\log d} f(p, t) \quad (72)$$

For late time, $f(p, t)$ curves toward its limiting value $f(p, \infty) = 1$, so that $S_{\text{vN}}(t)$ converges to its limiting value $\frac{L}{\log d}$, which is the von Neumann entropy of a maximally mixed state.

The $\log d$ dependence of the slope is different from the one predicted in Eq. (33). We believe it is a subtle difference between two architectures, see Eq. (76) and Eq. (78) for the difference in a 0-dimensional toy model.

In Fig. 7 we show the simulated results for bipartite entanglement measures. As a comparison and benchmark, for $p = 0$ unitary-only case Fig. 7(a), the mutual information grows and saturates to a volume law (proportional to $|A|$) plateau. Fig. 7(b) is part of Fig. 3(b) in the main text. It shows how $I(A, B)$ grows and reaches some peak value and then quickly decays to zero if $p \neq 0$. Fig. 7(d) is the result for the log-negativity. It behaves similarly as $I(A: B)$, indicating that the classical and the quantum parts of the correlation have qualitatively similar behavior.

B. Two dimension

We also performed simulation of a class of (2+1)D circuit to study whether our conclusion still holds in (2+1)D.

The circuit structure we simulated is displayed in Fig. 8(a, left): At each even (odd) time step, qubits in each blue (yellow) square are first acted by a random 4-qubit Clifford unitary gate with a probability 0.1, then acted by a 4-qubit trace channel with a probability $0.1p$. The pre-factor 0.1 appeared in both probabilities is meant to “slow down” the dynamics so that we can collect more data before the system fully thermalizes into a maximally mixed state. In each time step, unitary gates and measurements applied within different squares are independent of each other.

The system's geometry is shown in Fig. 8(a, right): the periodic boundary condition is taken in both spatial directions, while the region A and the region $B = \bar{A}$ are separated by a half-cut in the x-direction. Fig. 8(b) shows the mutual information between A and B , for various different L and p . It's clear from the plot that $I(A: B)$ scales linearly with the size of the boundary separating A and B , which is proportional to L .

VI. ONE QUDIT TOY MODEL

We consider a toy model with only one qudit (with Hilbert space dimension d). The purpose is to illustrate what to expect in the replica calculation and large d expansion.

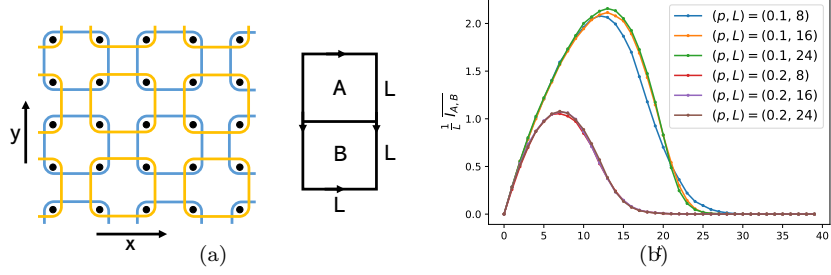


FIG. 8. (a, left) An illustration of the circuit structure and (a, right) the arrangement of A and B . See the text in Sec. V B for a detailed description. (b) Mutual information between A and B for various different p and L .

A. Random channel setup

At each step, we apply a random quantum channel $\Phi(\cdot) = (1 - p)U \cdot U^\dagger + \frac{p}{d}\mathbb{I}$ to the qudit. After t steps, the state will be:

$$(1 - p)^t U \rho_0 U^\dagger + \frac{1 - (1 - p)^t}{d} \mathbb{I}, \quad (73)$$

where $U = U_t \cdots U_2 U_1$ is again a random unitary and ρ_0 is a pure state.

The Rényi- n entropy is:

$$\frac{1}{1 - n} \log \text{tr}(\rho^n) = \frac{1}{1 - n} \log \left\{ \left[(1 - p)^t + \frac{1 - (1 - p)^t}{d} \right]^n + (d - 1) \left[\frac{1 - (1 - p)^t}{d} \right]^n \right\}. \quad (74)$$

The von Neumann entropy is:

$$-\text{tr}(\rho \log \rho) = - \left[(1 - p)^t + \frac{1 - (1 - p)^t}{d} \right] \log \left[(1 - p)^t + \frac{1 - (1 - p)^t}{d} \right] - (d - 1) \frac{1 - (1 - p)^t}{d} \log \frac{1 - (1 - p)^t}{d}. \quad (75)$$

Taking the large d limit, the Rényi- n entropy becomes:

$$\frac{nt}{1 - n} \log(1 - p) + o(1), \quad (76)$$

and the von Neumann entropy becomes:

$$[1 - (1 - p)^t] \log d - (1 - p)^t \log(1 - p)^t - [1 - (1 - p)^t] \log[1 - (1 - p)^t] + o(1). \quad (77)$$

We see that two limits $n \rightarrow 1$ and $d \rightarrow \infty$ do not commute. Therefore, with large d expansion, one cannot calculate the von Neumann entropy by replica trick [namely, taking the limit of $n \rightarrow 1$ in Eq. (76)]. The best thing one can do is the Rényi- n entropy with $n > 1$.

B. Probabilistic trace setup

We apply the trace with probability p at each step. Then after t steps, the system remains is pure with probability $(1 - p)^t$ and is maximally mixed with probability $1 - (1 - p)^t$.

The averaged Rényi- n entropy and von Neumann entropy are equal:

$$\frac{1}{1 - n} \overline{\log \text{tr}(\rho^n)} = [1 - (1 - p)^t] \log d, \quad (78)$$

while the logarithmic of averaged partition function is:

$$\frac{1}{1 - n} \log \overline{\text{tr}(\rho^n)} = \frac{1}{1 - n} \log \left[(1 - p)^t + \frac{1 - (1 - p)^t}{d^{n-1}} \right]. \quad (79)$$

Taking the large d limit, it becomes:

$$\frac{t}{1-n} \log(1-p) + o(1). \quad (80)$$

We see that the average over trajectories and the logarithmic do not commute.

- [1] Tianci Zhou and Adam Nahum, “Emergent statistical mechanics of entanglement in random unitary circuits,” *Phys. Rev. B* **99**, 174205 (2019).
- [2] Benoît Collins and Piotr Śniady, “Integration with respect to the haar measure on unitary, orthogonal and symplectic group,” *Communications in Mathematical Physics* **264**, 773–795 (2006).
- [3] Sergey Bravyi, David Fattal, and Daniel Gottesman, “Ghz extraction yield for multipartite stabilizer states,” *Journal of Mathematical Physics* **47**, 062106 (2006).